

How to Incorporate Higher-order Interactions in Analog Ising Machines

Robbe De Prins^{1,2}, Guy Van der Sande², Peter Bienstman¹, and Thomas Van Vaerenbergh³

¹Photonics Research Group, Ghent University – imec, Technologiepark-Zwijnaarde 126,
9052 Gent, Belgium

²Applied Physics Research Group, Vrije Universiteit Brussel, Pleinlaan 2, 1050 Brussels,
Belgium

³Large-Scale Integrated Photonics Lab, Hewlett Packard Labs, HPE Belgium, Diegem,
Belgium

Abstract

Ising machines (IMs) are specialized devices designed to efficiently solve combinatorial optimization problems. Among such problems, Boolean Satisfiability (SAT) is particularly relevant in industrial applications. To solve SAT problems using IMs, it is crucial to incorporate higher-order interactions. However, in analog IMs, interactions of different orders scale unevenly with the continuous spin amplitudes, introducing imbalances that can significantly degrade performance. We present a numerical comparison of methods to mitigate these imbalances, evaluating time-to-solution and success rate on Uniform Random 3-SAT instances from the SATLIB benchmark set. Our results show that the most effective approach employs spin interactions that are proportional to the signs of spins, rather than their continuous amplitudes. This generalizes our previous work, which showed that such interactions best mitigate imbalances induced by external fields in quadratic analog IMs. In this work, its advantage becomes substantially more pronounced, as it naturally mitigates imbalances across all interaction orders. We further demonstrate that smooth approximations of this method make it compatible with analog hardware. Our findings underscore the central role of

spin-sign-based interactions in enabling robust and scalable analog IM dynamics.

1 Introduction

A broad spectrum of computational issues in science and industry can be formulated as combinatorial optimization problems (COPs). Among these, Boolean Satisfiability (SAT) problems are especially relevant to real-world industrial applications such as scheduling [1, 2], planning [3, 4], software and hardware verification [5–7], automatic test pattern generation [8, 9], and neurosymbolic AI [10, 11].

SAT’s practical importance is paralleled by its foundational complexity: it is widely believed that no algorithm can consistently solve all instances in polynomial time. In fact, SAT was the first problem proven to be NP-complete, as established by the Cook–Levin theorem [12, 13]. Consequently, a variety of heuristic and specialized methods have been developed to address SAT problems as efficiently as possible. Among these, Ising machines (IMs) have emerged as a class of promising candidates. These specialized physical or digital systems solve COPs by encoding them into an Ising model: a spin system

governed by the Hamiltonian

$$\mathcal{H}(\boldsymbol{\sigma}) = - \sum_i^N J_i^{(1)} \sigma_i - \sum_{i < j}^N J_{ij}^{(2)} \sigma_i \sigma_j, \quad (1)$$

where $\sigma_i = \pm 1$ ($1 \leq i \leq N$) denote the spins, and $J_i^{(1)}$ and $J_{ij}^{(2)}$ are the strengths of the external fields and pairwise couplings, respectively. The goal of the IM is to evolve toward low-energy configurations, which correspond to optimal or near-optimal solutions of the encoded COP.

Numerous IM implementations have been introduced to date [14]. For the purpose of this paper, we categorize them into two classes: IMs that are built using intrinsically binary spins $\sigma_i = \pm 1$ [15–18], and IMs employing continuous variables $s_i \in \mathbb{R}$ (e.g. intensities, voltages, etc.) [19–25]. Whereas the first group includes the bistability of the spins as a *hard constraint*, the latter group, which we will further refer to as analog IMs, implements this as a *soft constraint* [26].

To solve SAT problems directly on IMs, it is essential to incorporate *higher-order spin interactions* beyond the quadratic couplings of Eq. (1). In this work, we focus on 3-SAT problems, a canonical and prominent model for hard SAT instances, which naturally map to higher-order Ising Hamiltonians of the form:

$$\mathcal{H}(\boldsymbol{\sigma}) = - \sum_i^N J_i^{(1)} \sigma_i - \sum_{i < j}^N J_{ij}^{(2)} \sigma_i \sigma_j - \sum_{i < j < k}^N J_{ijk}^{(3)} \sigma_i \sigma_j \sigma_k, \quad (2)$$

where the coefficients $J_{i_1 \dots i_p}^{(p)}$ represent real-valued interaction strengths of order p . In the past, it has been shown that techniques that reduce higher-order terms to quadratic and linear interactions drastically impair the solver’s performance [27–31], underscoring the importance of incorporating these interactions natively.

However, incorporating higher-order spin interactions in *analog* IMs can be challenging. These difficulties arise from the dynamics governing the time evolution of the IM. For 3-SAT problems in particular, we will show in the next section that the time evolution of a spin amplitude s_i depends on terms of

the form

$$J_i^{(1)} + \sum_j J_{ij}^{(2)} s_j + \sum_{j < k} J_{ijk}^{(3)} s_j s_k. \quad (3)$$

Because interactions of different (polynomial) orders scale unevenly with the continuous spin amplitudes, their relative magnitudes can become unbalanced. In particular, if $s_i \ll 1$, the linear terms dominate the quadratic ones, which in turn dominate the cubic terms. This effect generalizes the imbalances between spin couplings and external fields observed in quadratic IMs [32–34], which we have shown to degrade the IM’s performance in prior work [35]. Here, this effect is amplified by the simultaneous presence of multiple interaction orders.

In this paper, we present a numerical comparison of methods aimed at mitigating such imbalances. We draw inspiration from existing analog higher-order IMs such as PolySimCIM [36], Hopf oscillator networks [28], and the higher-order simulated bifurcation algorithm [37]. Where possible, we also extend techniques that are common to address imbalances between external fields and quadratic spin interactions [32, 33]. To ensure a fair comparison, all methods are consistently implemented on an IM with identical, well-defined nonlinear dynamics that enforce spin bistability (details are provided in the next section) and with gradient-based spin dynamics (i.e. without momentum).

We benchmark the methods on Uniform Random 3-SAT instances from the SATLIB library [38], evaluating them in terms of time-to-solution (TTS) and success rate (SR). We find that spin-sign-based interactions—first introduced in discrete simulated bifurcation [21]—consistently yield superior performance for incorporating higher-order terms. These findings align with our previous work on quadratic Ising models [35].

While a previous study on the higher-order simulated bifurcation algorithm [37] reported reduced performance when applying the spin sign method, we hypothesize that this outcome stems from their exclusive focus on a purely third-order model (without quadratic and linear terms), where no imbalances arise between interaction orders. In a more realistic setting for SAT problems, where interactions

of multiple orders are included, we show that spin-sign-based interactions demonstrate a clear advantage, even more pronounced than in the setting with only quadratic couplings and external fields. Their ability to mitigate imbalances across all interaction orders highlights their critical role in designing effective analog IM dynamics. We reinforce this conclusion by demonstrating that these interactions can be implemented on analog hardware through smooth approximations.

2 Modeling analog Ising machines with higher-order spin interactions

Before introducing various techniques to incorporate higher-order spin interactions, we describe the analog IM that is used to benchmark them. The time evolution of spin amplitude $s_i \in \mathbb{R}$ is modeled as:

$$\frac{ds_i}{dt} = -s_i + \tanh(\alpha s_i + \beta I_i), \quad (4)$$

where α is the linear gain and β interaction strength. β follows a commonly used linear annealing scheme [39, 40] (see Methods for details). I_i represents the local field acting on s_i , whose exact form depends on how interactions of different orders are incorporated (this is discussed in the following section).

We use the hyperbolic tangent nonlinearity due to its strong empirical performance in previous work [41], which can be attributed to the suppression of amplitude inhomogeneity, a common source of performance degradation in IMs. Moreover, it reflects the saturation behavior that is commonly observed in experimental IMs [42].

The IM is simulated by numerically integrating Eq. (4) via the Euler-Maruyama method, which includes stochastic noise (see Methods for details). At any time during the simulation, the system's energy, as defined by the higher-order Hamiltonian of Eq. (2), can be evaluated by mapping the continuous spin amplitudes to binary spin values using a sign function: $\sigma_i = \text{sgn}(s_i)$.

2.1 Methods to incorporate higher-order interactions

We compare five approaches for incorporating higher-order interactions into analog IMs, each specifying a distinct form for the local field I_i in Eq. (4). These methods are applied to 3-SAT problems of the form of Eq. (2), but can be naturally extended to problems with interactions beyond third order.

Baseline method

As a baseline, we consider the following local field:

$$I_i = J_i^{(1)} + \sum_j J_{ij}^{(2)} s_j + \sum_{j < k} J_{ijk}^{(3)} s_j s_k. \quad (5)$$

This expression, also used in PolySimCIM [36] and in Coherent SAT Solvers [43], is a direct extension of the typical local field used, for example, in Coherent Ising machines [19]. It can be deduced from Eq. (2) by relaxing the binary spins σ_i to continuous variables $s_i \in \mathbb{R}$ and taking the negative of the partial derivative with respect to s_i .

When programming the IM, the coefficients $J_{i_1 \dots i_p}^{(p)}$ are carefully chosen to ensure that Eq. (2) encodes the intended COP (i.e. its ground state corresponds to the solution). However, this desired weighting among terms disappears when the spin amplitudes in Eq. (5) differ significantly from unity. In particular, if $s_i \ll 1$, the linear terms dominate the quadratic ones, which in turn dominate the cubic terms. Since such imbalances effectively discard information that is crucial to solving the COP, they can degrade the IM's performance. Note that the opposite case, where $s_i \gg 1$, is excluded, since we employ the tanh-nonlinearity of Eq. (4), which restricts the spin amplitudes within $[-1, 1]$.

Rescaling method 1

As a first way to address the imbalances between interaction orders, we propose the following expression:

$$I_i = J_i^{(1)} + \sum_j J_{ij}^{(2)} \frac{s_j}{\langle |s_m| \rangle} + \sum_{j < k} J_{ijk}^{(3)} \frac{s_j s_k}{\langle |s_m| \rangle^2}, \quad (6)$$

where $\langle |s_m| \rangle$ is the average absolute value of all spin amplitudes in the IM. This approach generalizes a technique originally proposed for purely quadratic IMs [32]. To the best of our knowledge, this extension has not been reported previously. By rescaling the spin amplitudes with $\langle |s_m| \rangle^{(-1)}$ and $\langle |s_m| \rangle^{(-2)}$, the scaling of the quadratic and cubic terms is adjusted to align with that of the linear terms $J_i^{(1)}$, preserving the intended balance among contributions.

Rescaling method 2

Alternatively, one can align the scaling of the linear and cubic terms with that of the quadratic couplings ($\propto J_{ij}^{(2)}$):

$$I_i = J_i^{(1)} \langle |s_m| \rangle + \sum_j J_{ij}^{(2)} s_j + \sum_{j < k} J_{ijk}^{(3)} \frac{s_j s_k}{\langle |s_m| \rangle}. \quad (7)$$

This expression is obtained from Eq. (6) by multiplying the entire local field by a global factor $\langle |s_m| \rangle$.

Rescaling method 3

By multiplying Eq. (7) once more by $\langle |s_m| \rangle$, we obtain:

$$I_i = J_i^{(1)} \langle |s_m| \rangle^2 + \sum_j J_{ij}^{(2)} s_j \langle |s_m| \rangle + \sum_{j < k} J_{ijk}^{(3)} s_j s_k, \quad (8)$$

which aligns the scaling of the linear and quadratic terms with the cubic terms ($\propto J_{ijk}^{(3)}$).

Spin sign method

Finally, we consider the following local field expression:

$$I_i = J_i^{(1)} + \sum_j J_{ij}^{(2)} \text{sgn}(s_j) + \sum_{j < k} J_{ijk}^{(3)} \text{sgn}(s_j) \text{sgn}(s_k). \quad (9)$$

It was originally proposed in the context of discrete simulated bifurcation [21, 37]. A similar approach for complex-valued spins represented by Hopf oscillators is proposed in Ref. [28]. In our previous work [35], we showed that this approach is effective at mitigating imbalances caused by external fields in quadratic IMs.

3 Results

3.1 Performance comparison

We benchmark the methods for incorporating higher-order interactions from Section 2.1 on Uniform Random-3-SAT problems from the SATLIB library (see Methods for details). Specifically, we consider the first 10 instances of each of the following SATLIB subsets: uf20-91, uf50-218, uf100-430, uf150-645, uf200-860, and uf250-1065. All of these instances are satisfiable, meaning the ground-state energy—used as the target for the TTS and SR metrics—corresponds to the situation where all boolean clauses are satisfied. As detailed in Methods, these performance metrics are computed by optimizing over the relevant hyperparameters of the IM.

Fig. 1 presents a pairwise comparison of the methods from Section 2.1 using the TTS metric. Each point represents a problem instance, with the y -value denoting the TTS of the spin sign method from Eq. (9), and the x -value denoting the TTS of the reference method.

Fig. 1(a) compares the spin sign method with the baseline method of Eq. (5). 54 of the 60 COPs lie below the diagonal, indicating that they are solved faster using the the spin sign method than using the baseline method. Notably, 4 of these 54 points fall in the grey region on the right, where $\text{TTS} = \infty$, meaning the baseline method could not solve them for any of the attempted hyperparameter values (see Methods for details) within the time limit $t_{\max} = 10^4$. In contrast, the spin sign method successfully solved all four, yielding finite TTS values.

Fig. 1(b) contrasts the spin sign method with rescaling method 1 of Eq. (6). In this comparison, the spin sign method outperforms on 59 of the 60 problems, with rescaling method 1 failing to solve 9 of them. The single instance where the spin sign method is slower lies nearly on the diagonal, indicating comparable performance.

Fig. 1(c) and (d) compare the spin sign method with rescaling methods 2 and 3, respectively. The spin sign method outperforms both across all instances. Rescaling method 2 fails to solve 7 of them, while rescaling method 3 fails on 4. Looking at

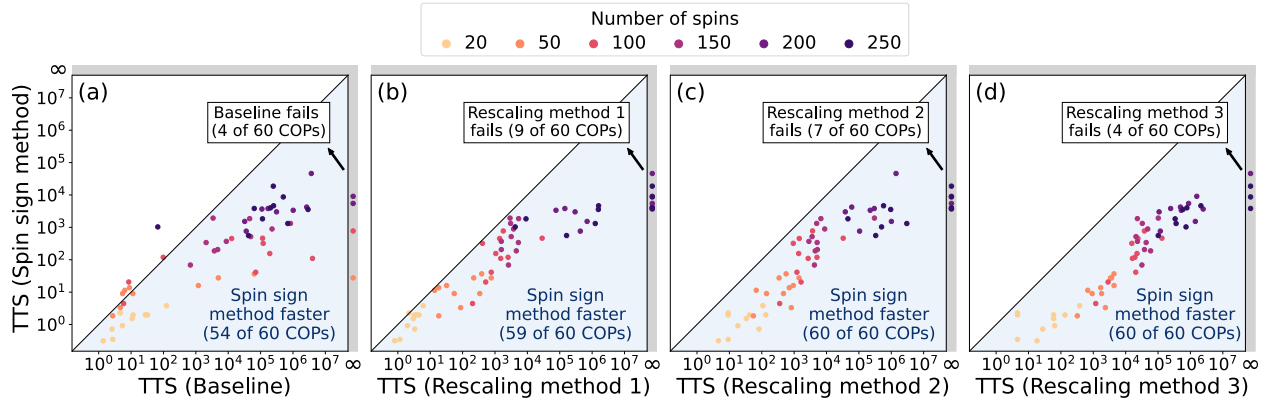


Figure 1: Comparison of TTS between the methods to incorporate higher-order interactions of Section 2.1 for Uniform Random-3-SAT problems. Dots in the grey area on the right denote COPs that could be solved by the spin sign method within the allocated compute time of $t_{\max} = 10^4$, but not by the method on the x-axis ($TTS = \infty$, $SR = 0$). The spin sign method generally requires less time to solve problems, and solves more problems within the allocated time. Details about the simulation procedure are provided in Methods.

Fig. 1(b-d) combined, we see a consistent pattern among the rescaling strategies. As seen from Eqs. (6) to (8), these models differ only by a global scaling factor $\langle |s_m| \rangle^q$ with $q \in \mathbb{Z}$. Increasing q (i.e. moving from method 1 to 2 to 3) tends to increase the average TTS for smaller instances (lighter dots), but improves performance on larger ones (darker dots), as reflected by a decrease in the number of unsolved problems ($TTS = \infty$). A possible explanation is that multiplying the local fields I_i by $0 \leq \langle |s_m| \rangle \leq 1$, and thus increasing q , slows down the IM dynamics, which may help avoid premature convergence in larger instances (which are generally harder) but becomes unnecessary overhead for smaller (generally easier) ones.

Combining the information from all panels from Fig. 1, the spin sign method shows clear advantages over the other four methods: it manages to solve more problems, and it generally yields lower TTS values. Notably, this advantage becomes more pronounced with increasing problem size. This trend is further confirmed in Fig. S3 of the Supplementary Material, which shows the TTS distributions for all methods as a function of problem size.

Detailed per-instance results underlying Fig. 1 are provided in Fig. S2 in the Supplementary Material. Additionally, while Fig. 1 uses a timestep of $dt =$

0.01 (see Methods), Fig. S4 presents a similar TTS analysis with a smaller timestep of $dt = 0.001$. The close agreement between the two confirms that $dt = 0.01$ is sufficiently small to accurately integrate the IM’s governing equations (Eq. (4)) for the problems that we studied.

We now confirm the advantage of the spin sign method over its alternatives using a second performance metric: the success rate. Instead of evaluating $\min_{\Theta} TTS$, we now consider $\max_{\Theta} SR$, where Θ denotes the set of hyperparameters (see Methods for details). Fig. 2(a) compares the SR of all methods across problem sizes. Each boxplot represents the SR distribution over 10 problem instances of the same size. We observe that all methods succeed at solving the problems of size 20 with near-perfect SR. However, as the problem size increases, the SR generally decreases. This decrease is slower for the spin sign method than for its alternatives. Fig. 2(b) visualizes the SR values relative to the spin sign method. We see that for almost all problems, the spin sign method yields equal or higher SR values than all other methods. Instance-specific data is provided in Fig. S1 of the Supplementary Material.

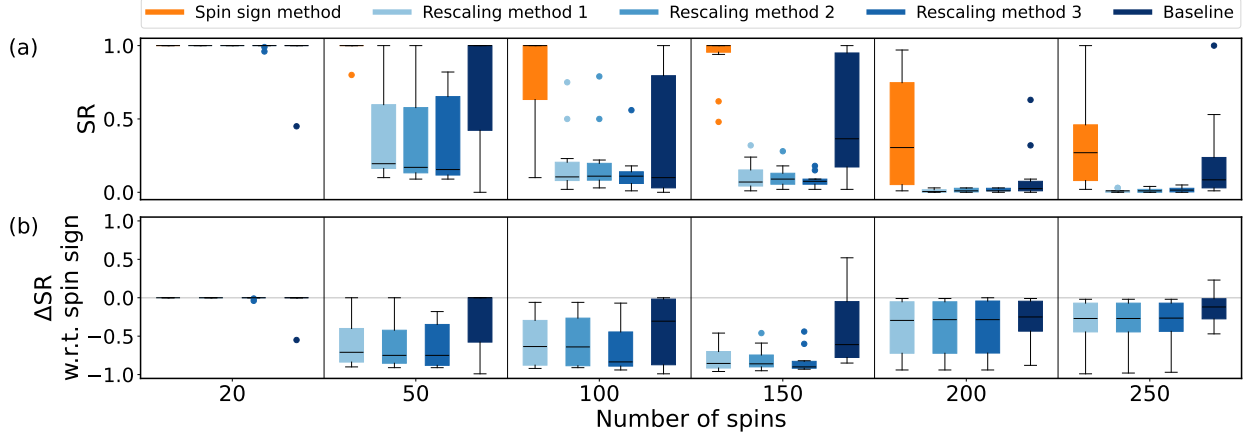


Figure 2: Comparison of success rates across the different methods to incorporate higher-order interactions of Section 2.1 on Uniform Random-3-SAT problems. Panel (a) shows absolute SRs, while panel (b) displays SRs relative to the spin sign method. Each boxplot represents a distribution over 10 instances of the same size for a given method, where dots indicate outliers. A detailed breakdown for individual problem instances is provided in Fig. S1 of the Supplementary Material.

3.2 Approximate spin sign method: simulating hardware-induced effects

When using the spin sign method of Eq. (9), the continuous spin amplitudes are mapped to their signs using the exact (discontinuous) sign function when computing local fields. While this works in simulation, physical implementations in analog hardware inevitably require a smooth approximation with finite steepness. To explore how this hardware-induced constraint affects performance, we introduce and evaluate a continuous approximation of the sign function:

$$\text{sgn}(s_i) \approx \tanh(\kappa s_i), \quad (10)$$

where the steepness parameter $\kappa \in \mathbb{R}$ controls the sharpness of the transition. For large κ , the approximation closely matches the exact sign function; smaller values yield more gradual transitions.

For varying values of κ , Fig. 3 shows the fraction of the benchmark problems that are solved fastest using each of the local field methods from Section 2.1. The curves sum to 1 at every value of κ . While only the approximate spin sign method depends on κ , changes

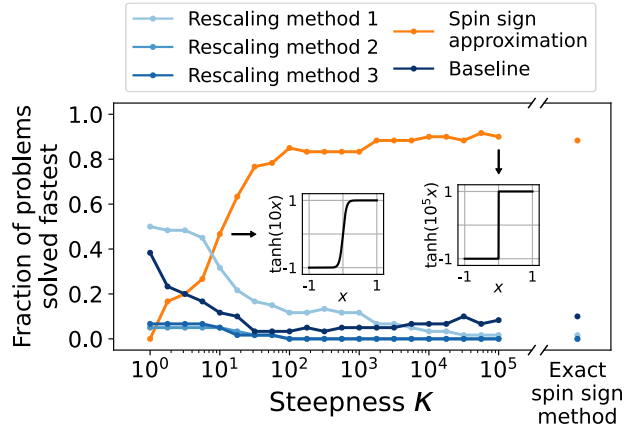


Figure 3: Fraction of benchmark problems for which each method is fastest, as a function of κ in the smooth $\tanh(\kappa s_i)$ approximation of the spin sign method. As the performance of the approximate method improves with increasing κ , the relative ranking across all methods shifts, eventually reaching the limit of the exact spin sign method.

in its performance affect the relative ranking of all methods. At $\kappa = 1$, we observe that the approximation is too smooth to be effective, and the method fails to outperform any alternative. As κ increases, the approximate spin sign method quickly improves. At $\kappa = 10$, it becomes the fastest method on the largest fraction of problems. As κ increases further, the performance converges toward that of the exact spin sign method.

4 Conclusion

We have benchmarked five methods for incorporating higher-order spin interactions into analog Ising machines. Our results show that the choice of local field formulation critically impacts performance, especially as problem size increases. While strategies that rescale the spin amplitudes with the mean absolute value of all spins partially mitigate amplitude imbalance and improve performance over the naive baseline, they are consistently outperformed by the spin sign method. This last method achieves higher success rates and lower time-to-solution across a wide range of problem sizes. Its performance also scales more favorably than the other methods, making it increasingly effective for larger problems.

These findings underscore the importance of maintaining balance among interaction terms for effective problem solving. Enforcing binary behavior in spin contributions to the local field helps preserve the problem’s discrete structure, leading to clear performance gains even in continuous-state dynamical systems. This serves as a key factor in advancing analog Ising machine architectures.

Beyond performance, the spin sign method offers notable practical advantages. As discussed in more detail in our previous work [35], this method is well-suited for hardware implementation. In many experimental IMs, spin amplitudes are already measured before computing local fields [19, 22–25, 44, 45], such that a simple one-bit comparator suffices to extract the spin sign. Whereas obtaining the sign of the spins is a local operation, calculating the average absolute spin value is a global operation over all spins, which is less trivial to implement. Additionally, in

this work, we showed that smooth approximations of the spin sign method, which arise naturally in analog hardware, can match the performance of the exact method, provided the approximation is sufficiently accurate.

This work focused on the local field formulation for higher-order interactions, keeping the dynamics of the analog IM fixed (cf. Eq. (4)). Future work could explore how modifying the dynamics—such as adding momentum terms to the gradient-based spin updates [21, 37] or incorporating chaotic amplitude control [43, 46, 47] — might further enhance performance. It would also be interesting to extend this comparison with higher-order IMs that employ phase variables, similar to the Kuramoto model [48].

Finally, comparing our approach against state-of-the-art SAT solvers is an important next step. While the direct TTS comparisons presented here effectively evaluate the local field methods from Section 2.1 within the analog IM framework, broader comparisons across fundamentally different algorithms and hardware require implementation-agnostic metrics. To this end, we can estimate the empirical time complexity of our solver [49, 50], which involves extensive benchmarking over a wider range of problem sizes and instance sets. Pursuing these directions will help assess the full potential of analog IMs for solving higher-order combinatorial problems.

5 Methods

5.1 Embedding SAT problems in a higher-order Ising model

The goal of a SAT problem is to find an assignment to a set of N Boolean variables such that a given logical formula evaluates to **True**. Every SAT problem can be expressed in conjunctive normal form (CNF) as a conjunction (logical AND, \wedge) of clauses, each of which is a disjunction (logical OR, \vee) of exactly L literals. A literal l is either a variable x_i or its negation $\neg x_i$. In the case of 3-SAT, we have $L = 3$.

A 3-SAT problem with C clauses can be expressed

as:

$$\bigwedge_{i=1}^C (\mathbf{l}_{i1} \vee \mathbf{l}_{i2} \vee \mathbf{l}_{i3}), \quad (11)$$

where \mathbf{l}_{ij} denotes the j -th literal in the i -th clause.

To embed a 3-SAT problem into the higher-order Ising Hamiltonian defined in Eq. (2), we first convert the logical formula into a real-valued PUBO energy function of binary variables $x_k \in \{0, 1\}$:

$$H(\mathbf{x}) = \sum_{i=1}^C (1 - l_{i1})(1 - l_{i2})(1 - l_{i3}), \quad (12)$$

where

$$l_{ij} = \begin{cases} x_k & \text{if the literal } \mathbf{l}_{ij} \text{ is } \mathbf{x}_k, \\ 1 - x_k & \text{if the literal } \mathbf{l}_{ij} \text{ is } \neg \mathbf{x}_k, \end{cases} \quad (13)$$

and $k \in \{1, \dots, N\}$. Note that every unsatisfied clause adds an energy penalty of +1 to Eq. (12).

We then express the energy function in terms of Ising spins $\sigma_i = \pm 1$ using the following transformation:

$$x_k = \frac{\sigma_k + 1}{2}. \quad (14)$$

5.2 Simulating the analog Ising machine

The temporal evolution of the Ising machine is modeled using the Euler–Maruyama integration method:

$$\mathbf{s}_{t+1} = \mathbf{s}_t + \Delta t (-\mathbf{s}_t + \tanh(\alpha \mathbf{s}_t + \beta_t \mathbf{I}_t)) + \gamma \boldsymbol{\xi}_t, \quad (15)$$

where \mathbf{s}_t denotes the vector of spin amplitudes at time t , α is the linear gain, and $\Delta t = 0.01$ is the time step (which is validated as detailed in the Supplementary Material). The local fields acting on the spins at time t are encoded in the vector \mathbf{I}_t , according to one of the methods of Section 2.1. γ denotes the noise strength, while each noise component $\xi_{t,i}$ is sampled independently from a normal distribution with zero mean and standard deviation $\sqrt{\Delta t}$. The interaction strength β_t is gradually increased over time using:

$$\beta_{t+1} = \beta_t + v_\beta \Delta t, \quad (16)$$

starting from $\beta_0 = 0$, with v_β denoting the annealing rate.

The initial values of the spin amplitudes are sampled from the same Gaussian distribution as the noise process, i.e. $\gamma \boldsymbol{\xi}_0$. The iterative updates of Eqs. (15) and (16) continue until the IM either achieves the target energy or completes $10^4/\Delta t$ steps.

For each problem instance, we perform a grid search over the hyperparameters, as detailed below. Each of the reported TTS values (e.g. in Fig. 1) corresponds to the optimal hyperparameter configuration identified through this process. For each hyperparameter setting, the IM evolution is repeated 100 times to estimate the TTS.

- Linear gain: $\alpha \in \{-10, -9, \dots, 1\}$
- Annealing speed:
 $v_\beta \in \{10^{-4}, 10^{-3}, 10^{-2}, 10^{-1}, 1\}$
- Noise strength: $\gamma \in \{10^{-4}, 10^{-3}, 10^{-2}, 10^{-1}\}$

6 Data availability

The authors declare that all relevant data are included in the manuscript. Additional data are available from the corresponding author upon reasonable request.

7 Author contributions

R.D.P. performed the simulations and wrote the manuscript. G.V.d.S., P.B., and T.V.V. supervised the project. All authors discussed the results and reviewed the manuscript.

8 Additional information

Competing interests: The authors declare no competing interests.

Acknowledgements: We would like to thank Adrien Renaudineau for his work on implementing the PUBO embeddings of SAT problems. This research was funded by the Horizon Europe framework (Prometheus project 101070195) and by the

Research Foundation Flanders (FWO) under grants G028618N, G029519N, G0A6L25N, and G006020N. Additional funding was provided by the EOS project ‘Photonic Ising Machines’. This project (EOS number 40007536) has received funding from the FWO and F.R.S.-FNRS under the Excellence of Science (EOS) programme. The work was also partly supported by the Defense Advanced Research Projects Agency (DARPA) under Air Force Research Laboratory (AFRL) contract no FA8650-23-3-7313.

References

- [1] Andrei Horbach, Thomas Bartsch, and Dirk Briskorn. Using a sat-solver to schedule sports leagues. *Journal of Scheduling*, 15:117–125, 2012.
- [2] Carla P Gomes, Bart Selman, Ken McAloon, and Carol Trethoff. Randomization in backtrack search: Exploiting heavy-tailed profiles for solving hard scheduling problems. In *AIPS*, pages 208–213, 1998.
- [3] Henry Kautz and Bart Selman. Pushing the envelope: Planning, propositional logic, and stochastic search. In *Proceedings of the national conference on artificial intelligence*, pages 1194–1201, 1996.
- [4] Stuart J Russell and Peter Norvig. *Artificial intelligence: a modern approach*. pearson, 2016.
- [5] Jerry R Burch, Edmund M Clarke, Kenneth L McMillan, David L Dill, and Lain-Jinn Hwang. Symbolic model checking: 1020 states and beyond. *Information and computation*, 98(2):142–170, 1992.
- [6] Armin Biere, Alessandro Cimatti, Edmund M Clarke, Masahiro Fujita, and Yunshan Zhu. Symbolic model checking using sat procedures instead of bdds. In *Proceedings of the 36th annual ACM/IEEE Design Automation Conference*, pages 317–320, 1999.
- [7] Miroslav N Velev and Randal E Bryant. Effective use of boolean satisfiability procedures in the formal verification of superscalar and vliw. In *Proceedings of the 38th annual design automation conference*, pages 226–231, 2001.
- [8] Haluk Konuk Tracy Larrabee et al. Explorations of sequential atpg using boolean satisfiability. In *VLSI Test Symposium 1993*, pages 85–90. Cite-seer, 1993.
- [9] Paul Stephan, Robert K Brayton, and Alberto L Sangiovanni-Vincentelli. Combinational test generation using satisfiability. *IEEE Transactions on Computer-Aided Design of Integrated Circuits and Systems*, 15(9):1167–1176, 2002.
- [10] Trieu H Trinh, Yuhuai Wu, Quoc V Le, He He, and Thang Luong. Solving olympiad geometry without human demonstrations. *Nature*, 625(7995):476–482, 2024.
- [11] Yunhao Yang, Neel P Bhatt, Tyler Ingebrand, William Ward, Steven Carr, Atlas Wang, and Ufuk Topcu. Fine-tuning language models using formal methods feedback: A use case in autonomous systems. *Proceedings of Machine Learning and Systems*, 6:339–350, 2024.
- [12] SA Cook. Proc. 3rd annu. acm symp. on theory of computing, 1971.
- [13] Frank J Balbach. The cook-levin theorem. *Archive of Formal Proofs*, 5:428, 2023.
- [14] Naeimeh Mohseni, Peter L McMahon, and Tim Byrnes. Ising machines as hardware solvers of combinatorial optimization problems. *Nature Reviews Physics*, 4(6):363–379, 2022.
- [15] Jan Kaiser and Supriyo Datta. Probabilistic computing with p-bits. *Applied Physics Letters*, 119, 2021. doi: <https://doi.org/10.1063/5.0067927>.
- [16] D Pierangeli, G Marcucci, and C Conti. Large-scale photonic ising machine by spatial light modulation. *Physical review letters*, 122(21):213902, 2019.

- [17] Fuxi Cai, Suhas Kumar, Thomas Van Vaerenbergh, Xia Sheng, Rui Liu, Can Li, Zhan Liu, Martin Foltin, Shimeng Yu, Qiangfei Xia, et al. Power-efficient combinatorial optimization using intrinsic noise in memristor hopfield neural networks. *Nature Electronics*, 3(7):409–418, 2020.
- [18] Mark W Johnson, Mohammad HS Amin, Suzanne Gildert, Trevor Lanting, Firas Hamze, Neil Dickson, Richard Harris, Andrew J Berkley, Jan Johansson, Paul Bunyk, et al. Quantum annealing with manufactured spins. *Nature*, 473(7346):194–198, 2011.
- [19] Toshimori Honjo, Tomohiro Sonobe, Kensuke Inaba, Takahiro Inagaki, Takuya Ikuta, Yasuhiro Yamada, Takushi Kazama, Koji Enbutsu, Takeshi Umeki, Ryoichi Kasahara, et al. 100,000-spin coherent ising machine. *Science advances*, 7(40):eabh0952, 2021.
- [20] Timothée Leleu, Yoshihisa Yamamoto, Peter L McMahon, and Kazuyuki Aihara. Destabilization of local minima in analog spin systems by correction of amplitude heterogeneity. *Physical review letters*, 122(4):040607, 2019.
- [21] Hayato Goto, Kotaro Endo, Masaru Suzuki, Yoshisato Sakai, Taro Kanao, Yohei Hamakawa, Ryo Hidaka, Masaya Yamasaki, and Kosuke Tatumura. High-performance combinatorial optimization based on classical mechanics. *Science Advances*, 7(6):eabe7953, 2021.
- [22] Fabian Böhm, Guy Verschaffelt, and Guy Van der Sande. A poor man’s coherent ising machine based on opto-electronic feedback systems for solving optimization problems. *Nature communications*, 10(1):3538, 2019.
- [23] L. Q. English, A. V. Zampetaki, K. P. Kalinin, N. G. Berloff, and P. G. Kevrekidis. An ising machine based on networks of subharmonic electrical resonators. *Communications Physics*, 5, 2022.
- [24] Mingrui Jiang, Keyi Shan, Chengping He, and Can Li. Efficient combinatorial optimization by quantum-inspired parallel annealing in analogue memristor crossbar. *Nature communications*, 14(1):5927, 2023.
- [25] Kirill P Kalinin and Natalia G Berloff. Global optimization of spin hamiltonians with gain-dissipative systems. *Scientific reports*, 8(1):17791, 2018.
- [26] Pedro Meseguer, Francesca Rossi, and Thomas Schiex. Soft constraints. In *Foundations of Artificial Intelligence*, volume 2, pages 281–328. Elsevier, 2006.
- [27] Dmitrii Dobrynin, Adrien Renaudineau, Mohammad Hizzani, Dmitri Strukov, Masoud Mohseni, and John Paul Strachan. Energy landscapes of combinatorial optimization in ising machines. *Physical Review E*, 110(4):045308, 2024.
- [28] Connor Bybee, Denis Kleyko, Dmitri E Nikonov, Amir Khosrowshahi, Bruno A Olshausen, and Friedrich T Sommer. Efficient optimization with higher-order ising machines. *Nature Communications*, 14(1):6033, 2023.
- [29] Elisabetta Valiante, Maritza Hernandez, Amin Barzegar, and Helmut G Katzgraber. Computational overhead of locality reduction in binary optimization problems. *Computer Physics Communications*, 269:108102, 2021.
- [30] Mohammad Hizzani, Arne Heitmann, George Hutchinson, Dmitrii Dobrynin, Thomas Van Vaerenbergh, Tinish Bhattacharya, Adrien Renaudineau, Dmitri Strukov, and John Paul Strachan. Memristor-based hardware and algorithms for higher-order hopfield optimization solver outperforming quadratic ising machines. In *2024 IEEE International Symposium on Circuits and Systems (ISCAS)*, pages 1–5. IEEE, 2024.
- [31] Giacomo Pedretti, Fabian Böhm, Tinish Bhattacharya, Arne Heitmann, Xiangyi Zhang, Mohammad Hizzani, George Hutchinson, Dongseok Kwon, John Moon, Elisabetta Valiante, et al.

- Solving boolean satisfiability problems with resistive content addressable memories. *npj Unconventional Computing*, 2(1):7, 2025.
- [32] Hiromasa Sakaguchi, Koji Ogata, Tetsu Isomura, Shoko Utsunomiya, Yoshihisa Yamamoto, and Kazuyuki Aihara. Boltzmann sampling by degenerate optical parametric oscillator network for structure-based virtual screening. *Entropy*, 18(10):365, 2016.
 - [33] Abhishek Kumar Singh, Kyle Jamieson, Peter L McMahon, and Davide Venturelli. Ising machines’ dynamics and regularization for near-optimal mimo detection. *IEEE Transactions on Wireless Communications*, 21(12):11080–11094, 2022.
 - [34] Sudeera Hasaranga Gunathilaka Mastiyage Don, Yoshitaka Inui, Satoshi Kako, Yoshihisa Yamamoto, and Toru Aonishi. Mean-field coherent ising machines with artificial zeeman terms. *Journal of Applied Physics*, 134(23), 2023.
 - [35] Robbe De Prins, Jacob Lamers, Peter Bienstman, Guy Van der Sande, Guy Verschaffelt, and Thomas Van Vaerenbergh. How to incorporate external fields in analog ising machines. *arXiv preprint arXiv:2505.08796*, 2025.
 - [36] Dmitry A Chermoshentsev, Aleksei O Malyshev, Mert Esencan, Egor S Tiunov, Douglas Mendoza, Alán Aspuru-Guzik, Aleksey K Fedorov, and Alexander I Lvovsky. Polynomial unconstrained binary optimisation inspired by optical simulation. *arXiv preprint arXiv:2106.13167*, 2021.
 - [37] Taro Kanao and Hayato Goto. Simulated bifurcation for higher-order cost functions. *Applied Physics Express*, 16(1):014501, 2022.
 - [38] H. Hoos and T. Stutzle. Satlib: An online resource for research on sat. In H. van Maaren I. P. Gent and T. Walsh, editors, *SAT2000*, pages 283–292. IOS Press, 2000.
 - [39] Atsushi Yamamura, Hideo Mabuchi, and Surya Ganguli. Geometric landscape annealing as an optimization principle underlying the coherent ising machine. *Phys. Rev. X*, 14:031054, 2024. doi: 10.1103/PhysRevX.14.031054.
 - [40] Jacob Lamers, Guy Verschaffelt, and Guy Van der Sande. Using continuation methods to analyse the difficulty of problems solved by ising machines. *Communications Physics*, 7, 2024.
 - [41] Fabian Böhm, Thomas Van Vaerenbergh, Guy Verschaffelt, and Guy Van der Sande. Order-of-magnitude differences in computational performance of analog ising machines induced by the choice of nonlinearity. *Communications Physics*, 4(1):149, 2021.
 - [42] Toon Sevenants. Using a spatial light modulator to achieve massive-parallelization in analog ising machines. Conference talk at the CLEO/Europe-EQEC, 2025.
 - [43] Sam Reifenstein, Timothee Leleu, Timothy McKenna, Marc Jankowski, Myoung-Gyun Suh, Edwin Ng, Farad Khoyratee, Zoltan Toroczka, and Yoshihisa Yamamoto. Coherent sat solvers: a tutorial. *Advances in Optics and Photonics*, 15(2):385–441, 2023.
 - [44] Takahiro Inagaki, Yoshitaka Haribara, Koji Igarashi, Tomohiro Sonobe, Shuhei Tamate, Toshimori Honjo, Alireza Marandi, Peter L McMahon, Takeshi Umeki, Koji Enbutsu, et al. A coherent ising machine for 2000-node optimization problems. *Science*, 354(6312):603–606, 2016.
 - [45] Natalia G Berloff, Matteo Silva, Kirill Kalinin, Alexis Askitopoulos, Julian D Töpfer, Pasquale Cilibrizzi, Wolfgang Langbein, and Pavlos G Lagoudakis. Realizing the classical xy hamiltonian in polariton simulators. *Nature materials*, 16(11):1120–1126, 2017.
 - [46] Timothée Leleu, Yoshihisa Yamamoto, Peter L McMahon, and Kazuyuki Aihara. Destabilization of local minima in analog spin systems by correction of amplitude heterogeneity. *Physical review letters*, 122(4):040607, 2019.

- [47] Timothée Leleu, Farad Khoyratee, Timothée Levi, Ryan Hamerly, Takashi Kohno, and Kazuyuki Aihara. Scaling advantage of chaotic amplitude control for high-performance combinatorial optimization. *Communications Physics*, 4(1):266, 2021.
- [48] Mohammad Khairul Bashar and Nikhil Shukla. Designing ising machines with higher order spin interactions and their application in solving combinatorial optimization. *Scientific Reports*, 13(1):9558, 2023.
- [49] Zongxu Mu and Holger H Hoos. On the empirical time complexity of random 3-sat at the phase transition. In *IJCAI*, pages 367–373, 2015.
- [50] Zongxu Mu. *Analysing the empirical time complexity of high-performance algorithms for SAT and TSP*. PhD thesis, University of British Columbia, 2015.

Supplementary Material

S.1 Success rates and time-to-solution for individual problem instances

Fig. S1 shows the success rate achieved on each individual Uniform Random-3-SAT instance, for each of the methods of Section 2.1. This breakdown highlights the variability across instances that is not visible in the aggregated boxplots of Fig. 2. Similarly, Fig. S2 shows the TTS values for individual problems and local field methods, underlying Fig. 1.

S.2 Distribution of time-to-solution across problem sizes

In Fig. 1 of the main text, we observed that data points increasingly diverge from the diagonal as problem size grows (indicated by darker dots). To make this trend more explicit, we show the TTS distribution for all methods from Section 2.1, grouped by problem size. As seen in Fig. S3, the spin sign method maintains lower TTS values than the alternative methods, with the performance gap widening as the number of spins increases.

S.3 Validation of time step size

As described in Section 5, all results in the main text were obtained using a time step of $dt = 0.01$. To ensure this choice is sufficiently small for accurately integrating the governing equations of the IM (Eq. (4)), we repeat the TTS analysis with a smaller time step of $dt = 0.001$. The results, shown in Fig. S4, closely match those in Fig. 1, confirming that $dt = 0.01$ yields reliable integration.

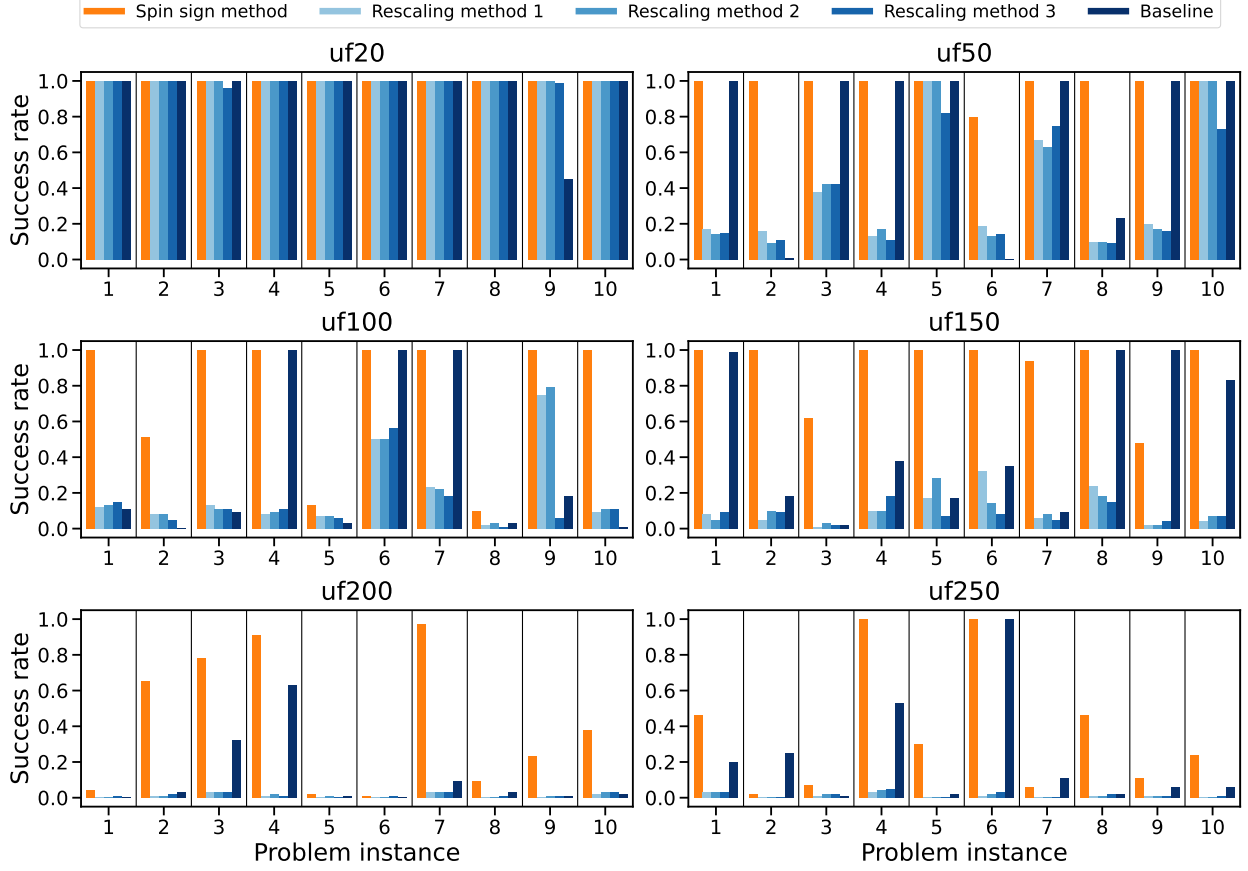


Figure S1: Instance-specific success rates for the Uniform Random-3-SAT instances, underlying the box-plots in Fig. 2. We compare the various methods to incorporate higher-order interactions, as described in Section 2.1. Problem names follow the format $uf\{N\}-\{i\}$, where N is the number of spin variables (indicated in the subplot title) and i is the instance identifier (shown along the x-axis).

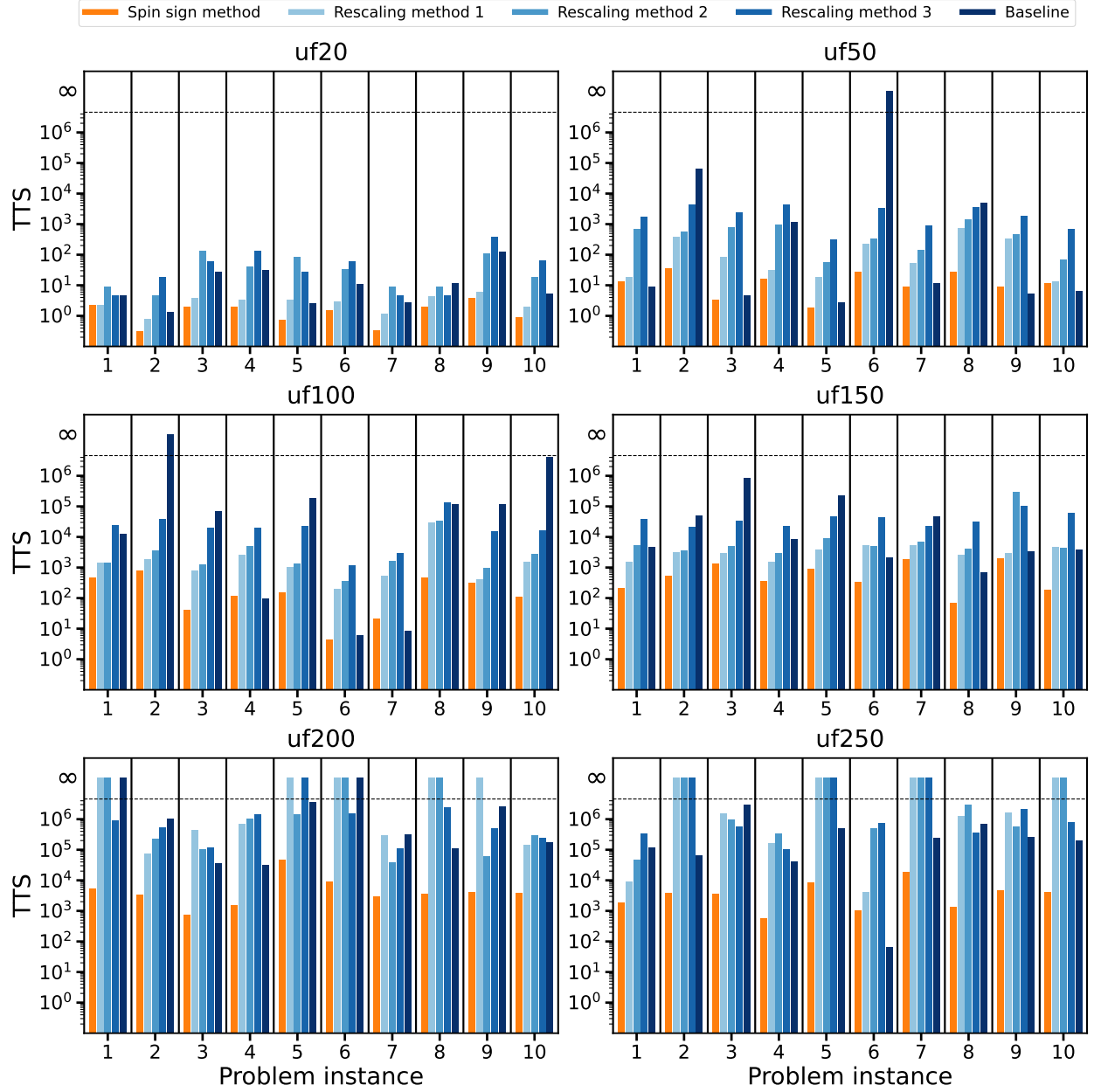


Figure S2: Instance-specific time-to-solution values for the Uniform Random-3-SAT instances, underlying Fig. 1. We compare the various methods to incorporate higher-order interactions, as described in Section 2.1. The dashed line denotes the resolution limit of the TTS metric. All bars surpassing this limit denote $TTS = \infty$, meaning they were not solved by the given method for any of the hyperparameter values (cf. Section 5). Problem names follow the format $uf\{N\}-\{i\}$, where N is the number of spin variables (indicated in the subplot title) and i is the instance identifier (shown along the x-axis).

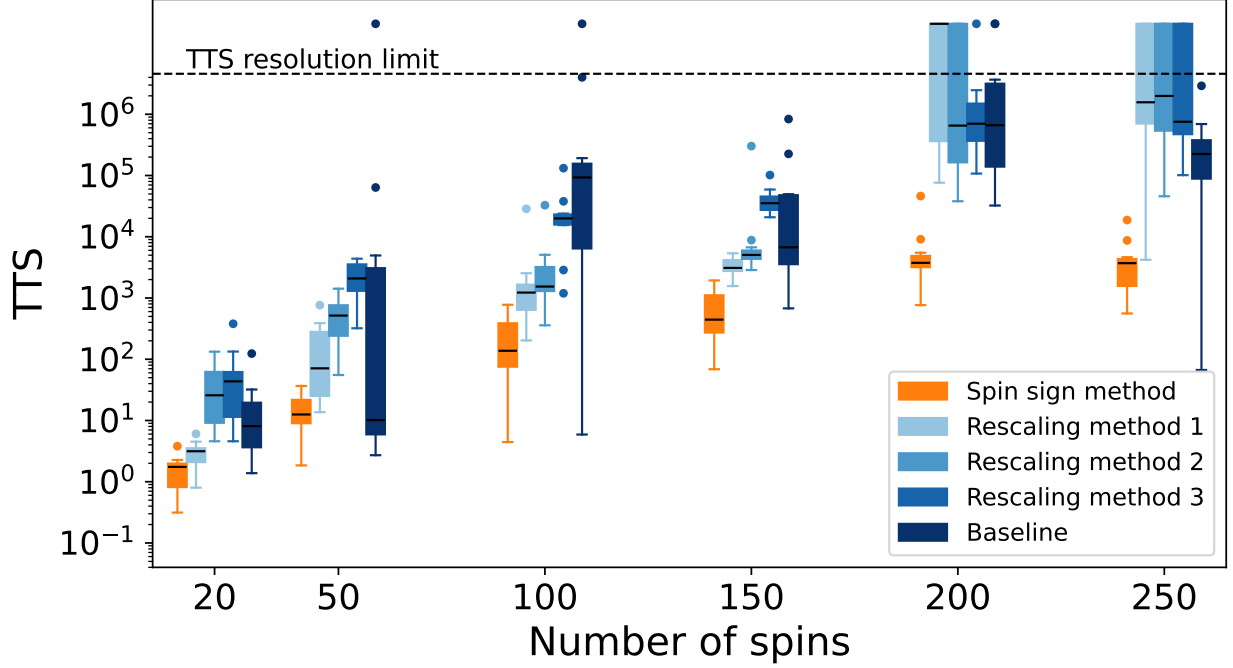


Figure S3: TTS distributions across problem sizes for all methods from Section 2.1. Each boxplot represents TTS values over 10 instances of the same size. Outliers are shown as dots. The advantage of the spin sign method over the alternative methods grows with increasing problem size.

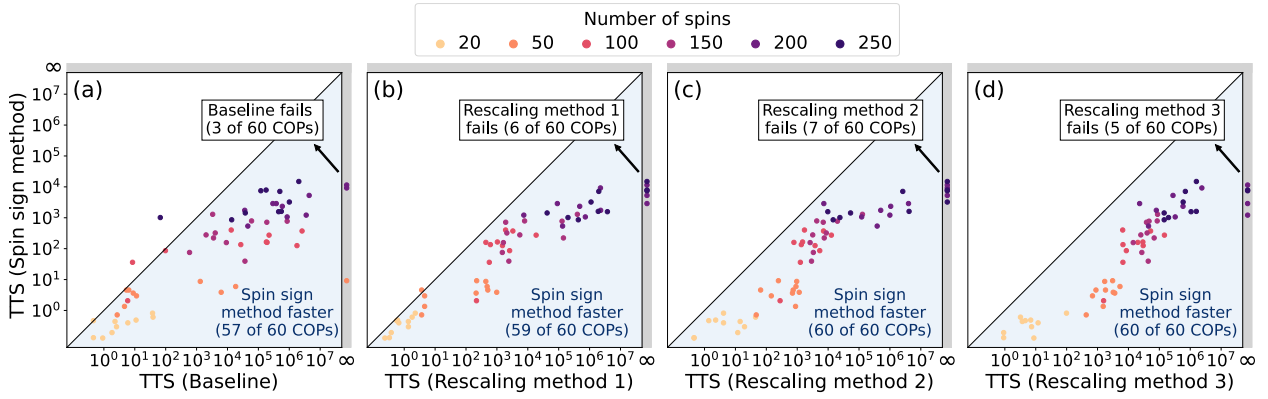


Figure S4: Comparison of TTS across methods for incorporating higher-order interactions (see Section 2.1) on Uniform Random-3-SAT instances. This figure mirrors Fig. 1 from the main text but uses a smaller timestep of $dt = 0.001$ instead of $dt = 0.01$. The similarity with Fig. 1 indicates that $dt = 0.01$ is sufficient for accurately integrating the IM's governing equations (Eq. (4)).